Singular Basis Functions and Curvilinear Triangles in the Solution of the Electric Field Integral Equation

William J. Brown and Donald R. Wilton, *Fellow, IEEE*

***Abstract*— Basis functions are formulated that account for singularities in the charge density near an edge on a conducting body. The formulation is general and the basis functions are valid for planar as well curvilinear geometries. In principle, singularities of any order can be treated, but best results are obtained for so-called "knife edge" singularities. Results are compared with exact solutions or measurements where available for some simple problems.**

***Index Terms*— Basis functions, boundary integral equations, curvilinear geometry.**

I. Introduction

SINCE the introduction of triangle surface-patch basis functions [1], triangular surface-patch modeling with the method of moments has become one of the most widely used techniques for solving electromagnetic scattering and radiation problems. This approach uses planar triangles to model the geometry and basis functions with a constant divergence to represent the surface current. The electric field integral equation (EFIE) is then solved via the method of moments. The use of planar triangles, however, can lead to unnatural discretization errors when surfaces with curvature are modeled.

Recently, several authors have introduced patches with curvature in an effort to circumvent this problem. A hybrid finite-element integral equation approach using curvilinear patches was employed by Antilla [2]. Improvement in radar cross section (RCS) values was shown by Wilkes and Cha [3] when solving the EFIE using curvilinear triangular patches. Ingber and Ott [4] studied the use of a "superparametric element" in the solution of the magnetic field integral equation (MFIE). Their method gave the geometry quadratic approximation and the current linear approximation. Cam *et al.* [5] used curvilinear patches and the MFIE to study Fabry–Perot cavities. A formulation for basis functions on curvilinear parametric patches was given by Wandzura [6]. Improved accuracy in the computation of resonant frequencies of spheres and cylinders was demonstrated by Zhu and Landstorfer [7] when using curvilinear quadrilateral and triangular patches.

Another deficiency of the basis functions of [1] is their inability to accurately model the charge density close to a sharp edge. It is well known that the charge density near an edge exhibits a singularity [8], [9]. Including this singularity in the basis functions can result in improved convergence, as shown by Richmond [10] in his study of scattering from a conducting strip grating. Wilton and Govind [11] showed that failure to include the edge behavior can lead to erroneous results near the edge for the case of TM scattering from a strip. Basis functions that account for edge singularities on surfaces were formulated by Andersson [12], but his analysis was limited to planar rectangular elements.

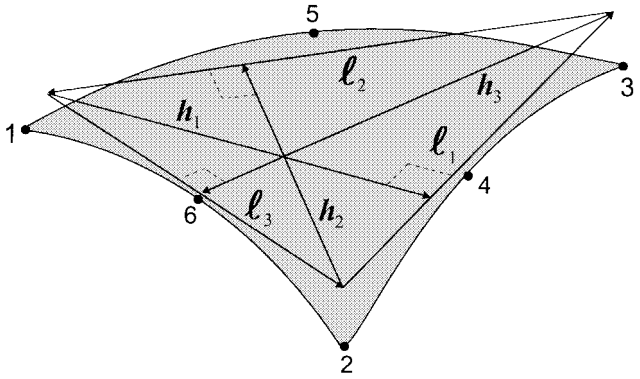

Fig. 1. Planar triangle tangent to curved triangle.

In Section II, a brief formulation is given for curvilinear triangles and the triangular basis function is defined. In Section III, the singular basis function for triangles is derived. The basis functions are used in the method of moments solution of the EFIE for planar as well as curvilinear geometries in Section IV, where their use in improving convergence and accuracy is demonstrated. Some results are given and limitations of the approach are illustrated.

II. Curvilinear Triangles and Nonsingular Basis Functions

A curvilinear triangle is shown in Fig. 1. Without lack of generality, a triangle may be assumed to be quadratic with six nodes interpolated by the quadratic functions

$$N_i(\xi_1,\xi_2,\xi_3)=\begin{cases}2\xi_i(\xi_i-\frac{1}{2}), & i=1,2,3\\ 4\xi_{i+1}\xi_{i-1}, & i=4,5,6,\end{cases} \tag{1}$$

where the indexes of the area coordinates ξ_i $(0\le\xi_i\le 1)$ are computed modulo three. A general point within a triangle with area coordinates (ξ_1,ξ_2,ξ_3) can be represented by

$$\boldsymbol{r}(\xi_1,\xi_2,\xi_3)=\sum_{i=1}^{6}\boldsymbol{r}_i N_i(\xi_1,\xi_2,\xi_3) \tag{2}$$

Manuscript received February 3, 1998; revised July 17, 1998.

W. J. Brown was with the Department of Electrical and Computer Engineering, University of Houston, Houston, TX 77204 USA. He is now with Raytheon Systems Company, El Segundo, CA 90245 USA.

D. R. Wilton is with the Department of Electrical and Computer Engineering, University of Houston, Houston, TX 77204 USA.

Publisher Item Identifier S 0018-926X(99)03721-7.

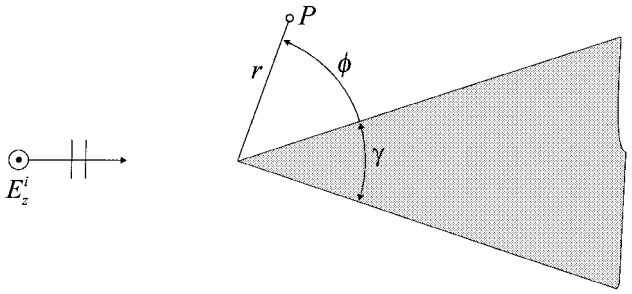

Fig. 2. Electric field incident on a metallic wedge.

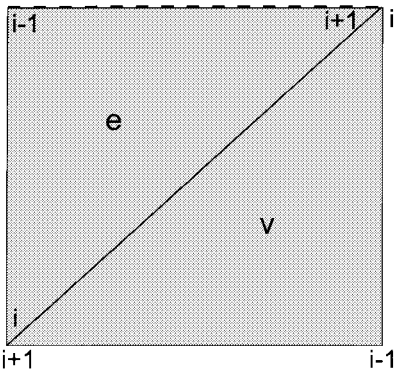

Fig. 3. Edge (e) and vertex (v) singularity triangles. The singularity is along the dashed line, which can be thought of as the *sharp* edge of a wedge-like structure. The local numbering scheme $(i, i+1, i-1)$ for the edge triangle is interior to the triangle while the scheme for the vertex triangle is exterior to the triangle.

where $\boldsymbol{r}_i$ is the vector from the origin to the ith node. At any point $\boldsymbol{r}_0$ in the curvilinear triangle, three tangent vectors $\boldsymbol{\ell}_i$ can be defined which constitute a planar triangle, tangent to the curvilinear triangle at $\boldsymbol{r}_0$. The surface *Jacobian* $\mathcal{J}$ is defined as

$$\mathcal{J} = |\boldsymbol{\ell}_1 \times \boldsymbol{\ell}_2| = |\boldsymbol{\ell}_2 \times \boldsymbol{\ell}_3| = |\boldsymbol{\ell}_3 \times \boldsymbol{\ell}_1| \tag{3}$$

and is equal to twice the area of the tangent triangle. A *locally* nonsingular defined basis function associated with the ith edge on an element E may be written as

$$\boldsymbol{\Lambda}_i^{\mathsf{E}}(\boldsymbol{r}) = \frac{\ell_i^c}{\mathcal{J}}(\xi_{i+1}\boldsymbol{\ell}_{i-1} - \xi_{i-1}\boldsymbol{\ell}_{i+1}) \tag{4}$$

where $\mathcal{J}$ is the Jacobian and ℓ_i^c is the magnitude of the length vector $\boldsymbol{\ell}_i$ at $\xi_{i+1} = \xi_{i-1} = \frac{1}{2}$. The locally defined index pair (E, i) may also be associated with the global curvilinear edge number n. From here on, the superscript E is understood and suppressed and the subscript denotes the local edge index. The factor ℓ_i^c normalizes the normal component of the flux density to unity at the midpoint of the edge. The divergence of this basis function is

$$\nabla \cdot \boldsymbol{\Lambda}_i^{\mathsf{E}}(\boldsymbol{r}) = \frac{2\ell_i^c}{\mathcal{J}}. \tag{5}$$

$\boldsymbol{\Lambda}_i^{\mathsf{E}}(\boldsymbol{r})$ is a divergence-conforming basis, meaning that it has continuous normal components of flux density across element boundaries. Equation (4) is a natural extension of the basis function derived in [1] and enjoys many of the same properties. Although the basis function contains linear terms, both it and its divergence are complete within the triangle only to order zero (with a weighting factor $\frac{1}{\mathcal{J}}$). In general, both the tangent vectors and the Jacobian vary with position inside the triangle.

III. Development of the Singular Basis Functions on Triangles

Consider the wedge shown in Fig. 2. It is well known that if the radius of curvature of the edge of the wedge is negligible compared to other local dimensions and to the wavelength of the incident wave, then the wedge can be modeled as *sharp*. This in effect removes one modeling parameter from the problem, namely, the radius of curvature of the edge. The simplification, however, leads to singularities in the fields of the model near the edge. It is argued in [11] that by using testing procedures which do not emphasize field values near edges, sufficient accuracy can often be obtained without modeling these singularities, but to obtain highly accurate solutions it is necessary to model these singular fields—especially in conjunction with higher order basis functions. The development of basis functions incorporating these singularities is detailed in this section. These singular bases accelerate the convergence of the solution and prevent deterioration of the solution near the model's edges.

The charge near an edge of a conducting object can be expanded in terms of order $\rho^{\alpha_n - 1}$ [9], where ρ represents distance from the edge of the wedge, tangent to the surface and

$$\alpha_n = n\pi/(2\pi - \gamma) \quad (n = 1, 2, \cdots) \tag{6}$$

where γ is the angle of the wedge. The dominant singularity is for the case $n = 1$ and the associated singularity exponent will henceforth be simply denoted as α. The smallest value of α is $\frac{1}{2}$, corresponding to a tangent wedge forming an infinite half plane $(\gamma = 0)$ or the so-called knife edge.

For curvilinear triangular patch modeling, only singularities of the following two types are allowed:

- edge singularities;
- vertex singularities.

Single triangles with a vertex at a surface corner and, therefore, having surface singularities along two edges are not allowed; such triangles are subdivided into two triangles, each with a single edge having a singularity. Consider the pair of triangles shown in Fig. 3. The edge with the heavy dashed line is considered to be an object edge. Hence, there exists an "edge" singularity along the ith edge (opposite the ith node) of triangle e and a "vertex" singularity at the ith node of triangle v. On triangle e the charge density will be proportional to $\xi_i^{\alpha-1}$, while for triangle v it is proportional to $(1 - \xi_i)^{\alpha-1}$.

The approach in the following sections is to derive basis functions by starting from the divergence of the basis functions and enforcing the correct behavior for the charge density. Thus, the basis functions should have the following properties.

1) Their surface divergence (i.e., charge density) should have the correct singular behavior.
2) As $\alpha \to 1$, they should reduce to the regular basis functions given in Section II.

3) They should have a bounded and continuous normal component at all edges.

These constraints ensure that proper basis functions for modeling edge behaviors are obtained.

A. Edge Singularities

The basis function associated with the ith edge of triangle e of Fig. 3 has the form

$$\boldsymbol{\Lambda}_i(\boldsymbol{r}) = C_i^e(\boldsymbol{\Omega}_i^+(\boldsymbol{r}) + \boldsymbol{\Omega}_i^-(\boldsymbol{r})) \tag{7}$$

where $\boldsymbol{\Omega}_i^{\pm}(\boldsymbol{r})$ interpolates the $\boldsymbol{\ell}_{i\mp1}$ vector component of the $i\pm1$ node and C_i^e is a normalization constant to be determined later. The interpolatory functions $\boldsymbol{\Omega}_i^{\pm}(\boldsymbol{r})$ have the form

$$\boldsymbol{\Omega}_i^{\pm}(\boldsymbol{r}) = \frac{1}{\mathcal{J}} f(\xi_i, \xi_{i\pm1})\boldsymbol{\ell}_{i\mp1} \tag{8}$$

where $f(\xi_i, \xi_{i\pm1})$ is a function to be determined and $\mathcal{J}$ is the Jacobian. Since the divergence of the basis function $\boldsymbol{\Lambda}_i$ is proportional to the charge density, the divergence of each interpolatory function $\boldsymbol{\Omega}_i$ is also proportional to the charge density. Consequently, the procedure for determining the unknown function f is to consider the divergence of each $\boldsymbol{\Omega}_i$ separately. The general expression for the surface divergence for a vector of the form $\boldsymbol{A} = \frac{1}{\mathcal{J}}(A_1\boldsymbol{\ell}_1 + A_2\boldsymbol{\ell}_2 + A_3\boldsymbol{\ell}_3)$ is given in [13] as

$$\nabla_s \cdot \boldsymbol{A} = \frac{1}{\mathcal{J}} \begin{vmatrix} 1 & 1 & 1 \\ \frac{\partial}{\partial \xi_1} & \frac{\partial}{\partial \xi_2} & \frac{\partial}{\partial \xi_3} \\ A_1 & A_2 & A_3 \end{vmatrix}. \tag{9}$$

Hence, the surface divergence of the function $\boldsymbol{\Omega}_i^-$ is written as

$$\begin{aligned} \nabla_s \cdot \boldsymbol{\Omega}_i^-(\boldsymbol{r}) &= \frac{1}{\mathcal{J}} \begin{vmatrix} 1 & 1 & 1 \\ \frac{\partial}{\partial \xi_i} & \frac{\partial}{\partial \xi_{i+1}} & \frac{\partial}{\partial \xi_{i-1}} \\ 0 & f(\xi_i, \xi_{i+1}) & 0 \end{vmatrix} \\ &= \frac{1}{\mathcal{J}} \frac{\partial f(\xi_i, \xi_{i+1})}{\partial \xi_i} \propto \frac{\xi_i^{\alpha-1}}{\mathcal{J}}. \end{aligned} \tag{10}$$

Integrating both sides of (10) with respect to ξ_i yields

$$f(\xi_i, \xi_{i+1}) \propto \xi_i^{\alpha} + g(\xi_{i+1}) \tag{11}$$

where $g(\xi_{i+1})$ is an arbitrary function. Since $\boldsymbol{\Omega}_i^-$ interpolates the $i-1$ vertex, it must vanish along edge $i-1$, (i.e., when $\xi_{i-1} = 0$ then $\boldsymbol{\Omega}_i^- = 0$ and, therefore, $f(\xi_i, \xi_{i+1})|_{\xi_{i-1}=0} = 0$). Along this edge, $\xi_i = 1 - \xi_{i+1}$ so $g(\xi_{i+1}) = -(1-\xi_{i+1})^{\alpha}$. Equation (8) is now shown to be

$$\boldsymbol{\Omega}_i^-(\boldsymbol{r}) = \frac{1}{\mathcal{J}}\left[\xi_i^{\alpha} - (1-\xi_{i+1})^{\alpha}\right]\boldsymbol{\ell}_{i+1}. \tag{12}$$

Similarly, the interpolation function of the $\boldsymbol{\ell}_{i-1}$ component at the $i+1$ vertex is obtained as

$$\boldsymbol{\Omega}_i^+(\boldsymbol{r}) = \frac{1}{\mathcal{J}}\left[-\xi_i^{\alpha} + (1-\xi_{i-1})^{\alpha}\right]\boldsymbol{\ell}_{i-1} \tag{13}$$

and, hence, (7) becomes

$$\begin{aligned} \boldsymbol{\Lambda}_i^e(\boldsymbol{r}) &= C_i^e(\boldsymbol{\Omega}_i^+(\boldsymbol{r}) + \boldsymbol{\Omega}_i^-(\boldsymbol{r})) \\ &= \frac{C_i^e}{\mathcal{J}}\left[\left(\xi_i^{\alpha} - (1-\xi_{i+1})^{\alpha}\right)\boldsymbol{\ell}_{i+1}\right. \\ &\quad \left. + \left(-\xi_i^{\alpha} + (1-\xi_{i-1})^{\alpha}\right)\boldsymbol{\ell}_{i-1}\right]. \end{aligned} \tag{14}$$

In order to ensure the continuity of the normal component of current at the edge, (14) must be normalized to unity at the edge node "midpoint" ($\xi_{i+1} = \xi_{i-1} = \frac{1}{2}$) by requiring that $\boldsymbol{\Lambda}_i^e \cdot \hat{\boldsymbol{h}}_i|_{\xi_{i\pm1}=\frac{1}{2}} = 1$ there. Thus, (14) becomes

$$\begin{aligned} \boldsymbol{\Lambda}_i^e(\boldsymbol{r}) &= \frac{2^{\alpha-1}\ell_i^c}{\mathcal{J}}\left[\left(\xi_i^{\alpha} - (1-\xi_{i+1})^{\alpha}\right)\boldsymbol{\ell}_{i+1}\right. \\ &\quad \left. + \left(-\xi_i^{\alpha} + (1-\xi_{i-1})^{\alpha}\right)\boldsymbol{\ell}_{i-1}\right] \end{aligned} \tag{15}$$

where the factor ℓ_i^c is $|\boldsymbol{\ell}_i|$ at the edge node.

Now consider the function interpolating the $\boldsymbol{\ell}_i$ component at vertex $i-1$, $\boldsymbol{\Omega}_{i+1}^+(\boldsymbol{r})$. The charge density is still proportional to $\xi_i^{\alpha-1}$ and, hence, the divergence of $\boldsymbol{\Omega}_{i+1}^+(\boldsymbol{r})$ is

$$\begin{aligned} \nabla_s \cdot \boldsymbol{\Omega}_{i+1}^+(\boldsymbol{r}) &= \frac{1}{\mathcal{J}} \begin{vmatrix} 1 & 1 & 1 \\ \frac{\partial}{\partial \xi_i} & \frac{\partial}{\partial \xi_{i+1}} & \frac{\partial}{\partial \xi_{i-1}} \\ f(\xi_i, \xi_{i-1}) & 0 & 0 \end{vmatrix} \\ &= \frac{1}{\mathcal{J}} \frac{\partial f(\xi_i, \xi_{i-1})}{\partial \xi_{i-1}} \propto \frac{\xi_i^{\alpha-1}}{\mathcal{J}}. \end{aligned} \tag{16}$$

Solving for f yields

$$f(\xi_i, \xi_{i-1}) \propto \xi_i^{\alpha-1}\xi_{i-1} + g(\xi_i). \tag{17}$$

Since $\boldsymbol{\Omega}_{i+1}^+$ is interpolatory at vertex $i-1$, $f(\xi_i, \xi_{i-1})$ must vanish at $\xi_{i-1} = 0$, therefore, $g(\xi_i) = 0$. Hence, the function is written as

$$\boldsymbol{\Omega}_{i+1}^+(\boldsymbol{r}) = \frac{\xi_i^{\alpha-1}\xi_{i-1}}{\mathcal{J}}\boldsymbol{\ell}_i. \tag{18}$$

Similarly, $\boldsymbol{\Omega}_{i-1}^-$ is easily found to be

$$\boldsymbol{\Omega}_{i-1}^-(\boldsymbol{r}) = -\frac{\xi_i^{\alpha-1}\xi_{i+1}}{\mathcal{J}}\boldsymbol{\ell}_i. \tag{19}$$

The remaining bases on the triangle are obtained via a similar procedure, yielding

$$\boldsymbol{\Omega}_{i-1}^+(\boldsymbol{r}) = \frac{\xi_i^{\alpha}}{\mathcal{J}}\boldsymbol{\ell}_{i+1} \tag{20}$$

and

$$\boldsymbol{\Omega}_{i-1}^-(\boldsymbol{r}) = -\frac{\xi_i^{\alpha}}{\mathcal{J}}\boldsymbol{\ell}_{i-1}. \tag{21}$$

Basis functions associated with the $i+1$ and $i-1$ edges can be formed by "averaging" these nodal interpolating functions, yielding

$$\begin{aligned} \boldsymbol{\Lambda}_{i+1}^e(\boldsymbol{r}) &= C_{i+1}^e(\boldsymbol{\Omega}_{i+1}^+(\boldsymbol{r}) + \boldsymbol{\Omega}_{i+1}^-(\boldsymbol{r})) \\ &= \frac{C_{i+1}^e}{\mathcal{J}}\left(\xi_i^{\alpha-1}\xi_{i-1}\boldsymbol{\ell}_i - \xi_i^{\alpha}\boldsymbol{\ell}_{i-1}\right) \end{aligned} \tag{22}$$

$$\begin{aligned} \boldsymbol{\Lambda}_{i-1}^e(\boldsymbol{r}) &= C_{i-1}^e(\boldsymbol{\Omega}_{i-1}^+(\boldsymbol{r}) + \boldsymbol{\Omega}_{i-1}^-(\boldsymbol{r})) \\ &= \frac{C_{i-1}^e}{\mathcal{J}}\left(\xi_i^{\alpha}\boldsymbol{\ell}_{i+1} - \xi_i^{\alpha-1}\xi_{i+1}\boldsymbol{\ell}_i\right) \end{aligned} \tag{23}$$

which are normalized to become

$$\boldsymbol{\Lambda}_{i+1}^e(\boldsymbol{r}) = \frac{2^{\alpha-1}\ell_{i+1}^e}{\mathcal{J}}\left(\xi_i^{\alpha-1}\xi_{i-1}\boldsymbol{\ell}_i - \xi_i^{\alpha}\boldsymbol{\ell}_{i-1}\right), \tag{24}$$

$$\boldsymbol{\Lambda}_{i-1}^e(\boldsymbol{r}) = \frac{2^{\alpha-1}\ell_{i-1}^e}{\mathcal{J}}\left(\xi_i^{\alpha}\boldsymbol{\ell}_{i+1} - \xi_i^{\alpha-1}\xi_{i+1}\boldsymbol{\ell}_i\right). \tag{25}$$

B. Vertex Singularities

Now consider the case where the singularity is placed at the vertex of the triangle. The charge density is modeled to be proportional to $(1-\xi_i)^{\alpha-1}$, although strictly speaking this is true only when the edge opposite the vertex singularity on triangle v is parallel to the singular boundary. This is a good approximation even if the opposite edge on v is *not* parallel to the singular boundary, since the main interest is modeling the singular behavior at the vertex, not so much the actual variation in charge density along the triangle. Indeed, the level of approximation is consistent with modeling the charges as only piecewise constant on the nonboundary triangles.

The same procedure applied in the previous section can also be used to obtain vertex singularity basis functions. The surface divergence of $\boldsymbol{\Omega}_i^-$ is now written as

$$\nabla_s \cdot \boldsymbol{\Omega}_i^-(\boldsymbol{r}) \propto \frac{(1-\xi_i)^{\alpha-1}}{\mathcal{J}}. \tag{26}$$

from which $\boldsymbol{\Omega}_i^-$ may be determined as

$$\boldsymbol{\Omega}_i^-(\boldsymbol{r}) = -\frac{1}{\mathcal{J}}(1-\xi_i)^{\alpha-1}\xi_{i-1}\boldsymbol{\ell}_{i+1}. \tag{27}$$

The other interpolation function is similarly found to be

$$\boldsymbol{\Omega}_i^+ = \frac{1}{\mathcal{J}}(1-\xi_i)^{\alpha-1}\xi_{i+1}\boldsymbol{\ell}_{i-1}. \tag{28}$$

Averaging these results as before, the normalized basis function associated with the ith edge for a vertex singularity triangle is thus found to be

$$\boldsymbol{\Lambda}_i^v(\boldsymbol{r}) = \frac{\ell_i^c}{\mathcal{J}}[(1-\xi_i)^{\alpha-1}\xi_{i+1}\boldsymbol{\ell}_{i-1} - (1-\xi_i)^{\alpha-1}\xi_{i-1}\boldsymbol{\ell}_{i+1}]. \tag{29}$$

Now consider the basis function associated with the $i+1$ edge. Following the earlier approach, one obtains a prospective basis function of the form

$$\frac{C_{i+1}^v}{\mathcal{J}}[(1-\xi_i)^{\alpha-1}\xi_{i-1}\boldsymbol{\ell}_i - (1-\xi_i)^{\alpha-1}\xi_i\boldsymbol{\ell}_{i-1}] \tag{30}$$

where C_{i+1}^v is the normalization constant. However, the surface divergence of (30) is

$$\frac{C_{i+1}^v}{\mathcal{J}}[(\alpha+1)(1-\xi_i)^{\alpha-1} - (\alpha-1)(1-\xi_i)^{\alpha-2}] \tag{31}$$

which contains an incorrect singularity due to the presence of the $(1-\xi_i)^{\alpha-2}$ term. In order to eliminate the unwanted $(1-\xi_i)^{\alpha-2}$ term in (31), (30) must be modified to become

$$\boldsymbol{\Lambda}_{i+1}^v(\boldsymbol{r}) = \frac{C_{i+1}^v}{\mathcal{J}}[((1-\xi_i)^{\alpha-1} + (\alpha-1)(1-\xi_i)^{\alpha-2}) \times \xi_{i-1}\boldsymbol{\ell}_i - (1-\xi_i)^{\alpha-1}\xi_i\boldsymbol{\ell}_{i-1}] \tag{32}$$

which has a surface divergence

$$\nabla_s \cdot \boldsymbol{\Lambda}_{i+1}^v(\boldsymbol{r}) = \frac{C_{i+1}^v(\alpha+1)}{\mathcal{J}\alpha}(1-\xi_i)^{\alpha-1} \tag{33}$$

having the correct singularity. Enforcing the unit current density constraint at the centroid of the curvilinear edge, (32) becomes

$$\boldsymbol{\Lambda}_{i+1}^v(\boldsymbol{r}) = \frac{2^{\alpha-1}\ell_{i+1}^c}{\mathcal{J}\alpha}[((1-\xi_i)^{\alpha-1} + (\alpha-1)(1-\xi_i)^{\alpha-2}) \times \xi_{i-1}\boldsymbol{\ell}_i - (1-\xi_i)^{\alpha-1}\xi_i\boldsymbol{\ell}_{i-1}]. \tag{34}$$

The basis function associated with the $i-1$ edge may be similarly obtained as

$$\boldsymbol{\Lambda}_{i-1}^v(\boldsymbol{r}) = \frac{2^{\alpha-1}\ell_{i-1}^c}{\mathcal{J}\alpha}[(1-\xi_i)^{\alpha-1}\xi_i\boldsymbol{\ell}_{i+1} - ((1-\xi_i)^{\alpha-1} + (\alpha-1)(1-\xi_i)^{\alpha-2})\xi_{i+1}\boldsymbol{\ell}_i]. \tag{35}$$

Equations (35) and (36) must satisfy the requirement that the normal component of current be continuous across the edge. As in Fig. 3, it is usual for an edge singularity triangle (e) to lie adjacent to a vertex singularity triangle (v). Consider the normal component of $\boldsymbol{\Lambda}_{i-1}^e$ along the common $i-1$ edge, which is

$$\boldsymbol{\Lambda}_{i-1}^e(\boldsymbol{r}) \cdot \hat{\mathbf{n}}_{i-1}^e|_{\xi_{i-1}=0} = \frac{2^{\alpha-1}\ell_{i-1}^c}{\ell_{i-1}|_{\xi_{i-1}=0}}\xi_i^{\alpha-1}. \tag{36}$$

The normal component of current of $\boldsymbol{\Lambda}_{i-1}^v$ along edge $i-1$ is

$$\boldsymbol{\Lambda}_{i-1}^v(\boldsymbol{r}) \cdot \hat{\mathbf{n}}_{i-1}^v|_{\xi_{i-1}=0} = \frac{2^{\alpha-1}\ell_{i-1}^c}{\ell_{i-1}|_{\xi_{i-1}=0}}(1-\xi_i)^{\alpha-1}. \tag{37}$$

Recalling that the local area coordinates ξ_i will vary in opposite directions on the two adjoining triangles, it is seen that (37) equals (38). A similar argument applies to edge $i+1$. Hence, there are no line charges along the common edge of an edge singularity triangle and a vertex singularity triangle. The various singular basis functions and the corresponding surface divergences are summarized in Table I.

The integration of the singular basis functions may be accomplished using a modification of the so-called bidirectional method, which transforms the integration over a triangle into an integration over a square [14]. The singularity at a triangle vertex or edge is transformed into a singularity over an edge of the square. The quadrature points and weight coefficients are determined in the square region using the Gauss–Legendre method along the nonsingular dimension and a Gauss–Jacobi method appropriate to the singularity along the other dimension. For convenience, the resulting quadrature points and weights which account for the singularity may be transformed back and the integration carried out over the triangular region. The procedure is essentially an adaptation of the Gauss–Radau method to functions with singularities at a triangle edge or vertex. Details of the integration of these functions in the context of the EFIE are given in [15].

IV. Results

In this section, results are presented which show how the singular basis functions can improve the convergence in geometries which contain singularities.

TABLE I
ZERO-ORDER SINGULAR BASIS FUNCTIONS ON TRIANGLES AND THEIR CORRESPONDING SURFACE DIVERGENCES

Singular Basis Functions	Surface Divergence
$\Lambda_i^e(\boldsymbol{r}) = \frac{2^{\alpha-1}\ell_i^c}{J}[(\xi_i^\alpha - (1-\xi_{i+1})^\alpha)\underline{\boldsymbol{\ell}}_{i+1} + (-\xi_i^\alpha + (1-\xi_{i-1})^\alpha)\underline{\boldsymbol{\ell}}_{i-1}]$	$\nabla_s \cdot \Lambda_i^e(\boldsymbol{r}) = \frac{2^{\alpha-1}\ell_i^c}{J}\xi_i^{\alpha-1}$
$\Lambda_{i+1}^e(\boldsymbol{r}) = \frac{2^{\alpha-1}\ell_{i+1}^c}{J}(\xi_i^{\alpha-1}\xi_{i-1}\underline{\boldsymbol{\ell}}_i - \xi_i^\alpha \underline{\boldsymbol{\ell}}_{i-1})$	$\nabla_s \cdot \Lambda_{i+1}^e(\boldsymbol{r}) = \frac{2^{\alpha-1}\ell_{i+1}^c(\alpha+1)}{J}\xi_i^{\alpha-1}$
$\Lambda_{i-1}^e(\boldsymbol{r}) = \frac{2^{\alpha-1}\ell_{i-1}^c}{J}(\xi_i^\alpha \underline{\boldsymbol{\ell}}_{i+1} - \xi_i^{\alpha-1}\xi_{i+1}\underline{\boldsymbol{\ell}}_i)$	$\nabla_s \cdot \Lambda_{i-1}^e(\boldsymbol{r}) = \frac{2^{\alpha-1}\ell_{i-1}^c(\alpha+1)}{J}\xi_i^{\alpha-1}$
$\Lambda_i^v(\boldsymbol{r}) = \frac{\ell_i^c}{J}\left[(1-\xi_i)^{\alpha-1}\xi_{i+1}\underline{\boldsymbol{\ell}}_{i-1} - (1-\xi_i)^{\alpha-1}\xi_{i-1}\underline{\boldsymbol{\ell}}_{i+1}\right]$	$\nabla_s \cdot \Lambda_i^v(\boldsymbol{r}) = \frac{\ell_i^c(\alpha+1)}{J}(1-\xi_i)^{\alpha-1}$
$\Lambda_{i+1}^v(\boldsymbol{r}) = \frac{2^{\alpha-1}\ell_{i+1}^c}{J\alpha}\left[\left((1-\xi_i)^{\alpha-1} + (\alpha-1)(1-\xi_i)^{\alpha-2}\right)\xi_{i-1}\underline{\boldsymbol{\ell}}_i - (1-\xi_i)^{\alpha-1}\xi_i\underline{\boldsymbol{\ell}}_{i-1}\right]$	$\nabla_s \cdot \Lambda_{i+1}^v(\boldsymbol{r}) = \frac{2^{\alpha-1}\ell_{i+1}^c(\alpha+1)}{J\alpha}(1-\xi_i)^{\alpha-1}$
$\Lambda_{i-1}^v(\boldsymbol{r}) = \frac{2^{\alpha-1}\ell_{i-1}^c}{J\alpha}\left[(1-\xi_i)^{\alpha-1}\xi_i\underline{\boldsymbol{\ell}}_{i+1} - \left((1-\xi_i)^{\alpha-1} + (\alpha-1)(1-\xi_i)^{\alpha-2}\right)\xi_{i+1}\underline{\boldsymbol{\ell}}_i\right]$	$\nabla_s \cdot \Lambda_{i-1}^v(\boldsymbol{r}) = \frac{2^{\alpha-1}\ell_{i-1}^c(\alpha+1)}{J\alpha}(1-\xi_i)^{\alpha-1}$

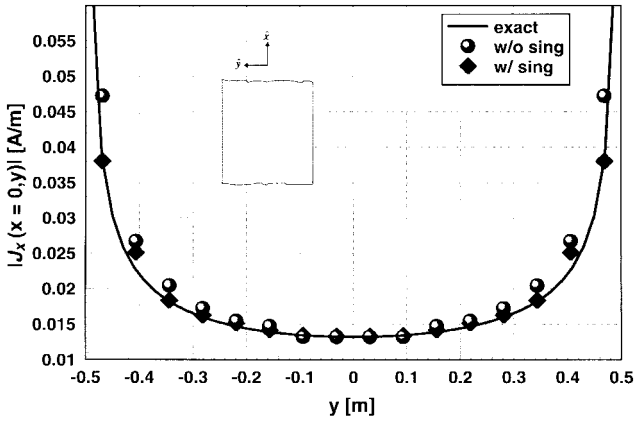

Fig. 4. The $\hat{\boldsymbol{x}}$-directed current at $x = 0$ for a long narrow strip. The electric field is incident from the $+\hat{z}$ direction and is polarized along $\hat{\boldsymbol{x}}$.

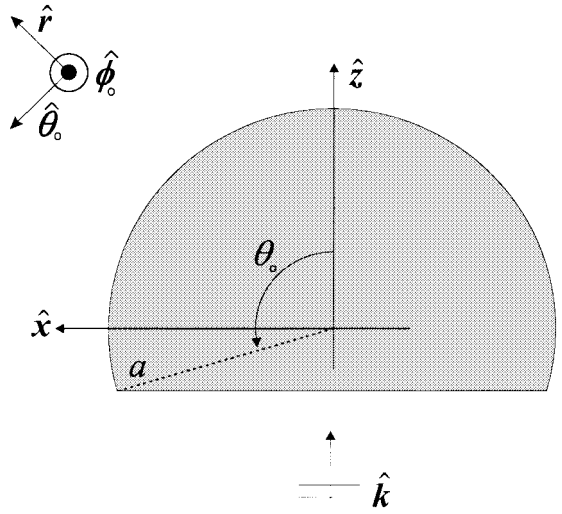

Fig. 5. Sphere with an aperture angle defined by $\pi - \theta_0$. A plane wave is incident from the $-\hat{z}$ direction.

A. Long Narrow Strip

The first example to be considered is the simple case of a long narrow strip (1λ in width, 10λ in length). The variation of the current across the narrow dimension of the strip is well approximated by that of an infinite strip. The strip lies in the xy plane with its axis along $\hat{\boldsymbol{x}}$. The electric field is polarized parallel to the axis of the strip and is incident from the $\hat{\boldsymbol{z}}$ direction. The "exact" curve in Fig. 4 is the current distribution for an infinite strip with singularities at the two edges that vary as the reciprocal square root of distance from the edge $\frac{C}{\sqrt{(\frac{1}{2})^2 - y^2}}$. The normalization constant C is set such that $2C = I_{\mathrm{MoM}}|_{x=0,y=0}$, where $I_{\mathrm{MoM}}|_{x=0,y=0}$ is the current given by the method of moments solution at $x = y = 0$. In all the remaining figures throughout the paper, "w/o sing" corresponds to the solution obtained when charge density singularities are not included, "w/ sing" is the solution with charge density singularities included. In Fig. 4, the current distribution across the strip at $y = 0$ is shown. Both solutions agree well with the exact solution near the center, but near the edges the solution without the singularity produces values that are roughly 30% greater than the exact value, as predicted in [11]. The solution with the edge singularity included agrees very well with the exact solution with some error apparently appearing in subdomains next to those containing singularities.

B. Sphere with Aperture

Consider the configuration shown in Fig. 5, which is modeled using quadratic curvilinear triangles. A thin, perfectly conducting spherical shell with an opening is represented by the surface $r = a$, $0 \le \theta \le \theta_0$ in the spherical coordinate system (r, θ, ϕ). The negative z axis passes through the center of the aperture, which has an opening angle defined as $\theta_{\mathrm{ap}} = \pi - \theta_0$. The medium inside and outside the shell is free-space.

Results are compared to those of Ziolkowski and Johnson [16]. In [16], a coupled TE and TM dual-series approach was used in which the singularity at the aperture was handled analytically. The approach required solving a small linear system of equations, the solution of which converged rapidly to produce highly accurate current and far field representations. Hence, the approach may be said to be semi-analytical. The results given in Fig. 6 are for the $\hat{\boldsymbol{\phi}}$-directed current at $\phi = \frac{\pi}{2}$ for a plane wave incident from the $-\hat{\boldsymbol{z}}$ direction with the electric field polarized along $\hat{\boldsymbol{\theta}}$. The aperture angle, θ_{ap}, is $\frac{\pi}{3}$ and $ka = 1$. As seen in the graph, when the charge density is not accounted for, the current near

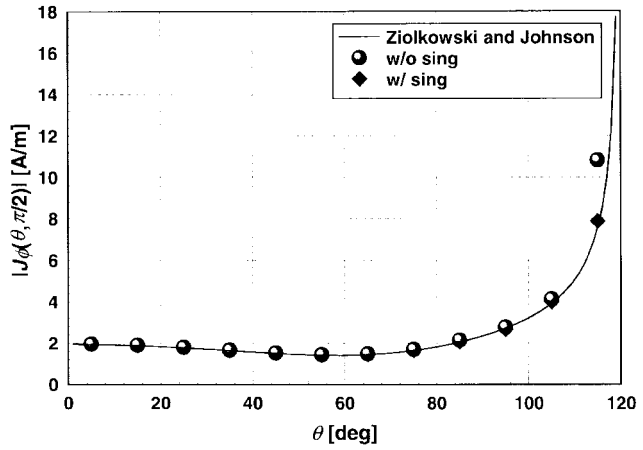

Fig. 6. The $\hat{\boldsymbol{\phi}}$-directed current at $\phi = \frac{\pi}{2}$ for a sphere with aperture $\theta_0 = 120°$.

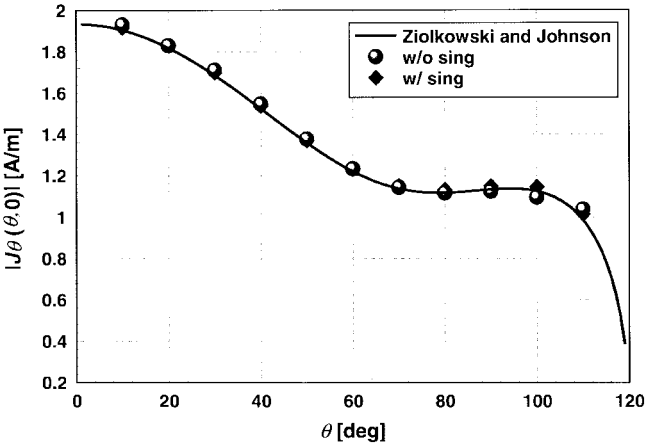

Fig. 7. The $\hat{\boldsymbol{\theta}}$-directed current at $\phi = 0$ for a sphere with aperture $\theta_0 = 120°$.

the aperture is roughly 30% higher than the solution of Ziolkowski and Johnson. When the singularity is included, very good agreement with the semi-analytical solution is achieved. Fig. 7 shows the $\hat{\boldsymbol{\theta}}$-directed current at $\phi = 0$ for the same polarization. Both solutions show roughly the same agreement with the semi-analytical solution. In both cases, 636 unknowns were used in the moment method solution. The solution with the charge singularity included required 869 central processing unit (CPU) seconds on a 166-Mhz DEC Alpha machine, while the solution without the charge singularity required 807 CPU seconds.

C. Triangular Cylinder

Both the previous examples had only knife-edge singularities for which $\alpha = \frac{1}{2}$. This case is special in that no current flows across the edge containing the singularity. It might appear that the basis functions derived earlier apply to any wedge angle and, therefore, any value of α. Now consider the case of the equilateral triangular cylinder given in Fig. 8. Each side of the cylinder cross section is 1 [m] in length while the length extends from $z = 16$ [m] to -16 [m]. The electric field is polarized along $\hat{\mathbf{z}}$ and is incident from the $\phi = 0$ direction with $ka = 1$ (where a is the base of the triangle). Since the angle between the faces of the triangle is 60°, α will equal $\frac{3}{5}$. The current is sampled in the middle of the cylinder at $z = 0$. Shown for reference is the current for a TM polarized plane wave incident on an infinite cylinder [17]. Good agreement is obtained along the BC face, on which the wave is incident. Along the two adjacent faces however, the surface patch results show the current leveling off at a higher level than that calculated for the infinite cylinder. Indeed, measured results by Iizuka and Yen [18] indicate that for a cylinder 12λ in length (2195 MHz), the current does level off at a rate only a bit slower than that predicted by the surface patch model. This particular example required over 2100 unknowns.

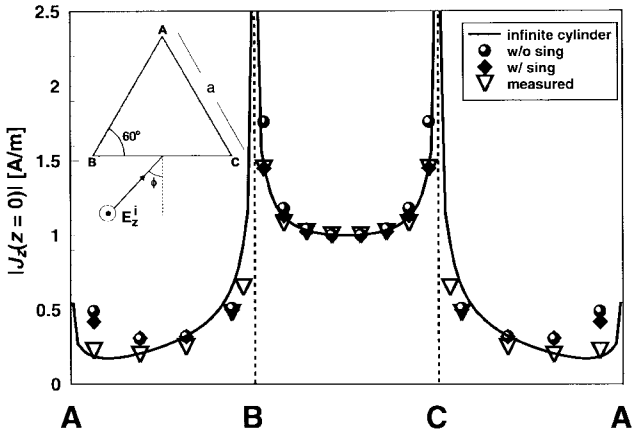

Fig. 8. Current at $z = 0$ for a triangular cylinder.

There is a possible difficulty in modeling singular currents that flow across edges, which likely accounts for the error seen in the triangular cylinder problem. Near an edge the component of magnetic field parallel to the edge behaves like

$$H_z \propto A + Br^{\alpha} \cos \alpha\phi \tag{38}$$

and, hence, the current normal to the edge behaves as

$$J_n = A \pm Br^{\alpha} \tag{39}$$

for current on surfaces $\phi = 0$, $\phi = \frac{\pi}{2\pi - \gamma}$, respectively. The second term produces the singularity in the charge; the first term is a divergence-free contribution representing an additional, independent degree of freedom. The divergence-free contribution cancels at a knife-edge when the oppositely-directed currents on the front and back sides of the surface are added to obtain a total equivalent current. The bases constructed in this paper actually contain terms having both forms, but they are *not* independent degrees of freedom. This will be investigated in a future paper.

V. Conclusion

New bases are developed that incorporate charge singularities into curvilinear triangular basis functions. For knife-like edges, the new bases demonstrate improved accuracy and convergence properties. For such edges, currents do not flow across the singular edge. Apparently the new basis functions contain an insufficient number of degrees of freedom to model

current components normal to an edge because independent degrees of freedom are required for modeling the nonsingular divergenceless part and the part with a singular divergence.

REFERENCES

[1] S. M. Rao, D. R. Wilton, and A. W. Glisson, "Electromagnetic scattering by surfaces of arbitrary shape," *IEEE Trans. Antennas Propagat.*, vol. AP-30, pp. 409–418, 1982.

[2] G. E. Antilla, "Radiation and scattering from complex three-dimensional geometries using a curvilinear hybrid finite element-integral equation approach," Ph.D. dissertation, Univ. California, 1993.

[3] D. Wilkes and C. C. Cha, "Method of moments solution with parametric curved triangular patches," in *Proc. IEEE Int. Symp. Antennas Propagat.*, 1991, pp. 1512–1515.

[4] M. S. Ingber and R. H. Ott, "Application of the boundary element method to the magnetic field integral equation," *IEEE Trans. Antennas Propagat.*, vol. 39, pp. 606–611, 1991.

[5] H. Cam, S. Toutain, P. Gelin, and G. Landrac, "Study of a Fabry–Perot cavity in the microwave frequency range by the boundary element method," *IEEE Trans. Microwave Theory Tech.*, vol. 40, pp. 298–304, 1992.

[6] S. Wandzura, "Electric current basis functions for curved surfaces," *Electromagn.*, vol. 12, no. 1, pp. 77–91, 1992.

[7] N. Y. Zhu and F. M. Landstorfer, "Application of curved parametric triangular and quadrilateral edge elements in the moment method solution of the EFIE," *IEEE Microwave Guided Wave Lett.*, vol. 3, pp. 319–321, 1993.

[8] J. Meixner, "The behavior of electromagnetic fields at edges," New York Univ., Rep. EM-72, New York, 1954.

[9] J. Van Bladel, *Singular Electromagnetic Fields and Sources*. New York: Oxford Univ. Press, 1991.

[10] J. H. Richmond, "On the edge mode in the theory of TM scattering by a strip or strip grating," *IEEE Trans. Antennas Propagat.*, vol. AP-28, pp. 883–887, 1980.

[11] D. R. Wilton and S. Govind, "Incorporation of edge conditions in moment method solution," *IEEE Trans. Antennas Propagat.*, vol. AP-25, pp. 845–850, 1977.

[12] T. Andersson, "Moment method calculations on apertures using singular basis functions," *IEEE Trans. Antennas Propagat.*, vol. 41, pp. 1709–1716, 1993.

[13] R. D. Graglia, D. R. Wilton, and A. F. Peterson, "Higher order interpolatory vector bases for computational electromagnetics," *IEEE Trans. Antennas Propagat.*, vol. 45, pp. 329–342, 1997.

[14] G. Dhatt and G. Touzot, *The Finite Element Method Displayed*. New York: Wiley, 1984.

[15] W. J. Brown, "Higher order modeling of surface integral equations," Ph.D. dissertation, Univ. Houston, Houston, TX, Dec. 1996.

[16] R. W. Ziolkowski and W. A. Johnson, "Electromagnetic scattering of an arbitrary plane wave from a spherical shell with a circular aperture," *J. Math. Phys.*, vol. 28, no. 6, pp. 1293–1314, 1987.

[17] S. V. Yesantharao, "EMPACK—A software toolbox of potential integrals for computational electromagnetics," Master's thesis, Univ. Houston, Houston, TX, Dec. 1989.

[18] K. Iizuka and J. L. Yen, "Surface currents on triangular and square metal cylinders," *IEEE Trans. Antennas Propagat.*, vol. AP-15, pp. 795–801, 1967.

William J. Brown was born in Grayson, KY, on September 3, 1966. He received the B.S. (physics) degree from the University of Kentucky, Lexington, in 1988 the M.S.E.E. from Florida State University, Tallahassee, in 1992, and the Ph.D. in electrical engineering from the University of Houston, Houston, TX, in 1996.

Currently, he is a Staff Engineer in the Electromagnetic Systems Laboratory at Raytheon Systems Company, El Segundo, CA. His research interests include microwave circuit design and computational electromagnetics.

Donald R. Wilton (S'63–M'65–M'70–SM'80–F'87), for a photograph and biography, see p. 315 of the March 1997 issue of this TRANSACTIONS.